

# Lidar-based Gust Load Alleviation - Results Obtained on a Generic Long Range Aircraft Configuration

Christian Wallace\*<sup>†</sup> and Nicolas Fezans\*

\*DLR (German Aerospace Center)

Lilienthalplatz 7, 38108 Braunschweig, Germany

christian.wallace@dlr.de · nicolas.fezans@dlr.de

<sup>†</sup>Corresponding author

## Abstract

In this paper a lidar-based preview gust load alleviation controller is synthesised via modern robust control methods in discrete time and optimised for an industrial long-range aircraft configuration. The synthesis and load analysis is performed using a set of 54 linear-time-invariant state-space models corresponding to a wide range of mass distributions and flight conditions. The controller performance is tested in a realistic hybrid and multi-rate simulation environment in which, in addition to the aeroelastic aircraft model (continuous time) and the various control functions in discrete time, the lidar measurement chain (sensor, wind estimation) as well as speed and position-limited actuators are simulated. The load alleviation performance is evaluated for a wide range of mass distributions, altitudes, airspeeds and gust lengths, leading to results based on over 4000 analysed gust load cases. The paper concludes with a discussion of the impact of the GLA control function on the structural loads, the load hierarchy and the general aircraft behaviour. The gust load alleviation controller achieves a reduction in peak bending moment between 17 % and 18 % at the important wing root, about 20 % in the middle of the wing and still over 10 % near the wing tip. It barely reaches the rate and position limits even on the extreme gusts defined in the certification specifications for large aeroplanes and only moderate increases of peak gust loads are observed on other load types or stations. Directly outside of the engine position a few percent increase in torsional moment is found. The controller yields an increase of about 50 % of the HTP gust loads, which is not critical as the HTP is usually, by far, not sized by gust loads but rather by manoeuvre loads. If needed, this figure could drastically be reduced by reducing the aggressiveness of the pitching behaviour and tolerating slight higher loads on the wing.

## 1. Introduction

### 1.1 Motivation

Society's expectations for a future clean and sustainable civil aviation are ambitious. In addition to the direct improvement of engine efficiency or the use of sustainable aviation fuel (SAF), the reduction of the aircraft net weight has always been an essential research objective in aeronautics. It reduces the required amount of lift, correspondingly the induced drag, and therefore the power or fuel consumption (correlating to both CO<sub>2</sub> and multiple non-CO<sub>2</sub> emissions). The structural design (and thereby the mass distribution) for the wings is mostly driven by inertia and aerodynamic loads. Aeroplanes in operational service are inevitably exposed to manifold loads. Beside the landing and manoeuvring loads, the aeroplane is also subject to external disturbances like turbulence and gusts.

A complete range of load case scenarios must be considered during an aircraft development programme, leading to complex sets of load hierarchies for each structural part of the aircraft as well as for each separate load component (e.g. bending moment). Even if other load types cannot be ignored and if manufacturing constraints may impose minimum thicknesses on some parts, significant portions of the primary wing root structure of typical modern CS 25 aircraft are often sized by gust load cases, particularly if a manoeuvre load alleviation (MLA) function has been already taken into account. The difference between the gust load envelope and the next type of loads is usually the load alleviation target that gust load alleviation (GLA) systems could help converting into weight savings, which has been known for decades [1, 2]. Active gust load alleviation is providing the opportunity to exploit potentials to modify and redistribute the wing lift distribution to lower structural loads dynamically, ideally considering the dynamic behaviour of the flexible structure.

## LIDAR-BASED GLA - RESULTS OBTAINED ON A GENERIC LONG RANGE AIRCRAFT CONFIGURATION

Active alleviation of gust loads is challenging and quite strongly limited by the available reaction time for the controller, considering the sensing of the gust or of its effect on the structure, delays in the loop, and the actuator bandwidth and rate limiters. Being able to sense the gust slightly in advance, typically 0.2 to 0.6 seconds before encountering it, drastically increases the reachable level of gust load alleviation, as already pointed out in [3,4]. Such anticipation could become possible with Doppler wind lidar sensors. Designing and building such sensors is challenging and this technology is still in development, but sensors with suitable characteristics for gust load alleviation could become available within the next decade.

## 1.2 Lidar-Based Feedforward Gust Load Alleviation

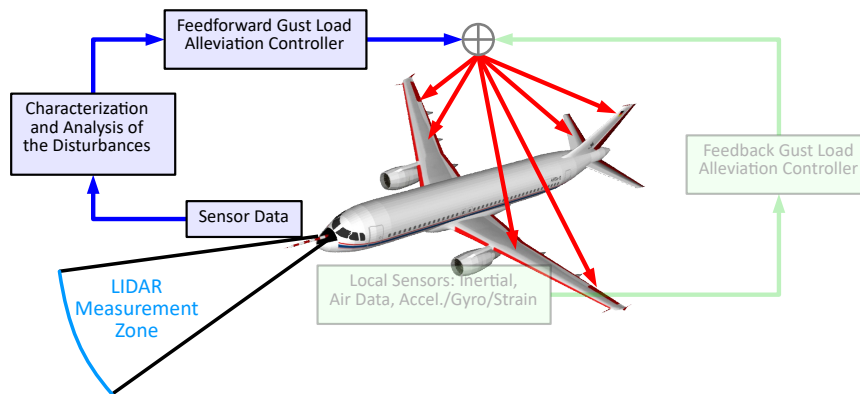


Figure 1: Schematic Illustration of Lidar-based Feedforward Control in Combination with Feedback Gust Load Alleviation (here unused and greyed out)

In contrast to a feedback gust load alleviation controller that uses sensors on the airframe to measure and react to the gust-induced aircraft response, a significantly higher load alleviation performance could be achieved by using optical lidar sensors to detect the atmospheric disturbances in advance. For this, a measurement zone ahead of the aeroplane is scanned permanently (Figure 1). However, the lidar measurements are relative velocities between sensor and molecules of the air in the so-called line-of-sight direction (laser beam axis). These measurements need to be combined to estimate the vertical wind ahead of the aircraft, which is done with a so-called wind reconstruction algorithm. The measurement process, the chosen lidar parameters (laser source, optics, detector, and scanning system) are not in the scope of the present paper. In this work, the solution presented in [5] is reused with some slight changes (e.g. maximum line-of-sight measurement range set to about 180 m).

Compared to those obtained from more classical air data sensors, the lidar-based vertical wind estimates are neither particularly precise nor well capturing the higher frequencies of the disturbances (above about 5-8 Hz) [6], but enable the feedforward GLA controller function to start taking control actions before changes in the aerodynamic loads occur. In addition to ailerons and/or spoiler deflections, pitching commands can be used to reduce the angle-of-attack variations due to the gust. Changing the angle of attack is extremely effective and efficient for modulating the aerodynamic forces, but very limited in terms of control bandwidth. Only very low frequency and low amplitude pitching commands can be used in practice due to their impact on the horizontal tailplane (HTP) and fuselage loads and to comfort considerations for passengers at the front and at the aft of the cabin. A dynamic lateral redistribution of the lift along the half of wingspan can also be performed simultaneously; considering the gust-induced aerodynamic response (including unsteady aerodynamic effects); the superimposed pitching motions that would result from the gust encounter and from the controller actions; the frequency response of the structure.

## 1.3 Relevant Prior Work

The consideration of lidar sensors for gust load alleviation is a rather specific topic for which only a fairly limited number of papers were published. A strong reference on the design and demonstration of direct-detection Doppler lidar for gust load alleviation come from the work performed by the Airbus group during the AWIATOR European project (see for instance [3] and references therein). Some groups, e.g. at JAXA [7,8], consider coherent lidar sensors which, however, rely on Mie scattering (instead of Rayleigh scattering). Coherent detection is simpler and easier than direct-detection, but requires aerosols which is a major problem for a gust load alleviation function, as it needs to operate at high altitude where the aerosol concentrations is often insufficient. Depending on the exact target pursued

## LIDAR-BASED GLA - RESULTS OBTAINED ON A GENERIC LONG RANGE AIRCRAFT CONFIGURATION

by the designer, e.g. enable lighter very high aspect ratio wings vs. improving passenger comfort, the requirements in terms of availability of the measurements would strongly differ. For other applications, especially at lower altitudes, the advantages of coherent lidar sensors prevail their disadvantages. Mendez et al. use similar ideas to reject the wind disturbances and alleviate the trajectory deviations resulting from them with a small quadcopter UAV. Such feedforward control concepts based on wind lidar measurements is also interesting for wind turbines [9–12]. For the control of wind turbines, such ideas could be used at scale earlier than for aircraft gust load alleviation, because of the easier atmospheric conditions, the longer time scales involved, and the lower constraints in terms of size, weight and power. One interesting observation made in [10, section 3.4] is that the feedback gains could be significantly reduced thanks to the feedforward disturbance rejection. This is, understandably, a typical result and trend when adding feedforward disturbance rejection to a closed-loop system (regardless of the system considered).

Regarding the design of aircraft gust load alleviation functions based on lidar measurements, two main groups can be distinguished: using model predictive control (MPC) [13, 14] or using frequency domain and/or robust control methods such as  $H_2$ ,  $H_\infty$ ,  $\mu$ -analysis techniques, see for instance [15, 16] or prior work of the authors. MPC provides a very natural way to consider information regarding the future gust provided by a lidar sensor and it is very easy to formulate such an MPC problem. However, such MPC controllers force to solve optimisation problems online which has a high computational burden and obtaining simultaneously strong stability guarantees and a bounded (and low enough) worst-case execution time is, to the best of the author's knowledge a problem that is not solved (and probably cannot be solved). The second category of methods forces to do significant more work upfront, but then provides controllers that pose no particular implementation and certification issues.

In recent years, various aspects linked to lidar-based gust load alleviation systems have been investigated by the authors as well as their research group and partners, see [17] and references therein. The work performed includes investigation on the processing of lidar sensor measurements [4, 6, 18] and sensitivity studies to determine the required performance, accuracy, etc. for use in feedforward gust load alleviation [6] as well as the optimal tuning of the wind reconstruction algorithm used [6]. Various aspects related to the optimal tuning of such lidar-based gust load alleviation functions have been also investigated, see for instance [19] for the consideration of the wind estimation performance directly in the controller synthesis, [5] and references therein for the overall tuning methodology, or [20] for the multi-fidelity assessment strategies of complex active gust load alleviation architectures. All this prior work and the related experience gained form the basis of the work presented.

#### 1.4 Scope and Structure of the Paper

This paper builds on the prior work mentioned above and focuses on the application to a twin engine generic long range aircraft configuration, which is representative of an industry-size load alleviation control design problem. The design, optimisation, and tuning of the lidar sensor and of the measurement processing chain is out of the scope of this paper, even if, compared to the work presented in [6], some parameters were adjusted to better fit the needs of this aircraft in terms of measurement range and critical gust lengths. Apart from the different aircraft configuration, some of the model processing steps, performance evaluation tools, and controller internal structure are also new compared to the authors' prior work.

Section 2 describes the considered application, the models, the main evaluation environment, and the considered gust load cases. Section 3 presents the controller design methodologies, the chosen controller structure, and tuning. Finally, sections 4 and 5 respectively present the results and conclusions of this work.

## 2. Considered Aircraft Configuration and Multi-Rate Evaluation Environment

This section presents the Generic Long Range Aircraft (GLRA) model that is considered in this work and the way the gust load envelope is defined and evaluated.

### 2.1 Considered Long Range Configuration and Aeroelastic Model

The Generic Long Range Aircraft (GLRA) is a wide-body twin-jet long-range research aircraft configuration. It features a classical wing (each wing is equipped with four independent ailerons) retrofitted with a large winglet (including an additional control surface called winglet tab) and downer and having an aspect ratio of about 9.5. Due to the need to use the GLRA for detailed flight simulations and/or as a realistic platform for controller development purposes, the configuration is represented by a very detailed aircraft model composed by the DLR modelling approach called VarLoads [21]. The integration of the model has been performed by the colleagues of the DLR Institute of System Dynamics and Control, which also have developed VarLoads, on the basis of the structural model provided by the DLR Institute of Aeroelasticity.

## LIDAR-BASED GLA - RESULTS OBTAINED ON A GENERIC LONG RANGE AIRCRAFT CONFIGURATION

A database-driven approach is used to generate the operating empty mass model, which consists of masses for the primary structure, the secondary structure, systems and equipment. Dependent on the particular mass case, the basic mass model is supplemented by specific additional payload and/or fuel masses. The structural stiffness is represented by a finite element model which is statically reduced to component-based loads reference axes as proposed by Guyan [22]. The reduced finite element model could be combined several times with the database-driven approach for the mass models to generate multiple design mass cases. This flexible process enables to generate manifold mass and centre of gravity combinations which allow to comply with certification rules like CS 25.321 [23].

The modelling of the aeroelastic aircraft is based on the so-called “mean-axes formulation” [24]. This approach consists of non-linear Newton-Euler equations of motion for the rigid body part which are coupled with linear modal equations of motion for the structural dynamics part. The linear modal equations are resulting from a transformation of the reduced stiffness model including the attached masses to its modal representation. Both the rigid and the elastic model part are excited by propulsion and aerodynamic forces. The aerodynamic loads are derived by applying an unsteady panel method based on potential flow theory, namely the doublet lattice method (DLM). The DLM calculates the aerodynamic matrices at discrete reduced frequencies. To use this data for time domain simulations a so-called rational function approximation (RFA) is used, which allows the unsteady aerodynamic model to be cast in state space form. The integrated or cut loads are recovered by the so called force summation method (FSM) [25]. This modelling approach [21, 26] has been used successfully for multiple applications [20, 27–31].

Nine different mass distributions were used for the GLA controller development (see Figure 2a). The available mass cases consist of a wide range of total masses and locations for the centre of gravity. The names of the mass cases used hereafter follow a specific nomenclature and are mentioned to ease comparison with other documents (internal as well as other existing or future publications), even though their exact meaning and the nomenclature used are not important for the work presented. The mass range varies between a lightweight mass case equivalent to the operational empty mass case (MOOee), cases (MCFfe and MCAae) which are slightly heavier (including some payload) or noticeable heavier (MHFFe and MHAAe, both with additional payload), a case with full payload (MZmMe), and cases with additional fuel (MTFFJ, MTAAJ and MTmMG, based on MHFFe, MHAAe and MZmMe) which are close or equivalent to the maximum take-off mass. The locations of the centre of gravity are varying between a more forward position (MCFfe, MHFFe and MTFFJ) and a more rearward position (MCAae, MHAAe and MTAAJ).

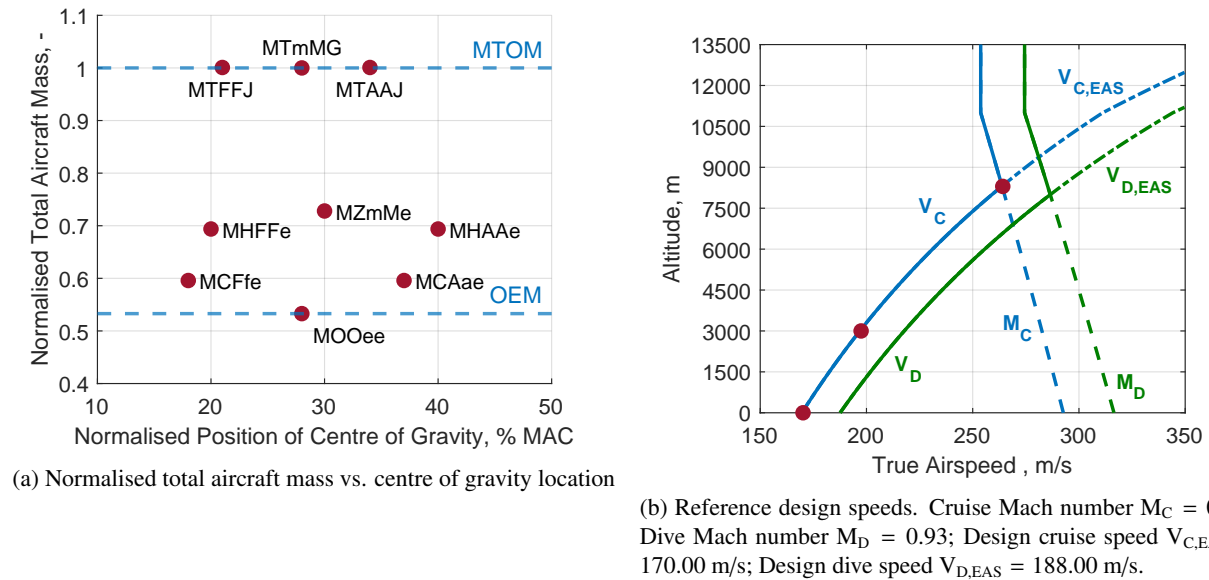


Figure 2: Design Flight Points and Design Mass Cases for GLA Controller Development (red dots)

The described modelling approach leads to a different non-linear model for each mass case. Each mass case-dependent model was trimmed at different flight points and linearised at the corresponding trim conditions. The flight points considered are combinations of three flight altitudes (0 m, 3000 m and 8300 m), all considered at the specific design cruise speed  $V_C$  (according to the certification rule CS 25.335 [23]) and represented with red dots in Figure 2b. For different flight altitudes,  $V_C$  corresponds to different true airspeeds and/or Mach numbers.

Three flight points corresponding to three different true airspeeds and Mach numbers were chosen based on a preliminary loads analysis (see Figure 2b). Additionally, *airbrake-out* cases are considered as well: for each combination of mass case and flight point, the same trim and linearisation process as for the *clean wing* configuration (i.e. only

## LIDAR-BASED GLA - RESULTS OBTAINED ON A GENERIC LONG RANGE AIRCRAFT CONFIGURATION

horizontal stabiliser deflection) is performed with constant  $35^\circ$  deflection of all spoilers. The difference between the *airbrake-out* and *clean wing* conditions is that the airbrakes reduce the total lift, which needs to be compensated by a higher angle-of-attack. This changes the lift distribution along the wing, the torsional moment along wing, and therefore the flight shape. This also changes the local lift increases that a gust would induce and so the dynamic response of the aircraft. In terms of active load alleviation, this also means that spoiler deflections cannot be used to reduce the gust loads when these spoilers are already fully deflected. Apart from worries that the use of dynamic spoiler deflections in the gust load alleviation function might lead to trigger buffeting effects, the fact that the peak gust load envelope is defined by *airbrake-out* cases for some parts of the wing motivated the investigation of the load alleviation potential when not using the spoilers for gust load alleviation.

Overall, 54 different aeroelastic models are available (cf. Table 1). Each linear model provides flight mechanical parameters like position, velocities, angular rates and air data parameters consisting of angle-of-attack and angle-of-sideslip (airspeed is assumed constant for the short duration of the simulations). Each linear model has 36 inputs for the control surfaces: i.a. eight different ailerons, two winglet tabs, six flaps, and a total of 12 spoilers. The wind inputs are defined through 50 different planes distributed along and perpendicular to the fuselage axis. For each plane, the normalised vertical wind velocity (normalised by dividing it with the true airspeed) and its time-derivative are required. This results in  $50 \cdot 2 = 100$  wind inputs in total. The structural model contains over 400 distributed structural points to monitor cut loads, resulting in over 2500 cut load outputs (3 forces and 3 moments for each point). Over 4800 outputs are used to display velocities and accelerations at various distributed locations on the flexible aircraft structure. Each linear aeroelastic state-space model has about 2800 states.

Table 1: Overview of Linear Aeroelastic Aircraft Models Available for GLA Controller Development

Mass Cases	Design Flight Points				Trim Conditions	Wing Conditions
	Altitude	Design Speed	True Airspeed	Mach Number		
MCAae MCFfe MHAAe MHFFe	0.0 m	$V_C$	170.00 m/s	0.50	steady- horizontal- flight	clean airbrake out
MOOee MTAAJ MTFFJ	3000.0 m	$V_C$	197.34 m/s	0.60		
MTmMG MZmMe	8300.0 m	$V_C$	264.26 m/s	0.86		

## 2.2 Simulation and Evaluation Environment

A realistic modular hybrid and multi-rate simulation environment [20] is used to simulate the various gust encounters and thereby assess the load alleviation performance. This environment is the most demanding but also the most powerful and precise evaluation environment being available for the authors' for load alleviation controller development and assessment. Simplified and faster simulation environments might be used at different stages of the control design and tuning (cf. later on the lower-right corner of Figure 4 or in [20]), but the final assessment is always performed with the most representative environment.

This environment consists of MATLAB<sup>®</sup> and Simulink<sup>®</sup> components as well as C++ code. Simulink<sup>®</sup> allows the integration and the coupling of various components (sub-models) from different sources to model complex systems. The numerical solvers provided with Simulink<sup>®</sup> allow the simulation of continuous-time, discrete-time, and hybrid<sup>1</sup> systems. Figure 3 is illustrating the overall structure of the environment, as it is used in the present work. All parts of the environment are presented schematically. The continuous-time components being represented by the light-blue blocks and the discrete-time components being represented with the other colours (each colour representing a different rate). The environment consists of the linear aeroelastic aircraft model (reconfigured CT-FOM, see evaluation workflow in Figure 4) and actuator models, composing the aeroservoelastic sub-model, a lidar sensor simulation, an online wind reconstruction algorithm to interpret the lidar measurements, and the control functions. The different systems/functions run with the correct rate: the flight physics run in continuous time, the flight control computer with different partitions (typically 25 and 100 Hz), the wind reconstruction at 10 Hz, and the lidar at its own much faster rate (1 kHz).

To enhance the accuracy of the simulation, the Simulink<sup>®</sup>-based evaluation environment is including generic non-linear actuator models for each control surface. The generic non-linear actuator models are second-order systems with dynamically adjustable parameters (angular frequency, damping, gain) and with position, rate, and accelerations

<sup>1</sup>i.e. involving both continuous-time and discrete-time elements

## LIDAR-BASED GLA - RESULTS OBTAINED ON A GENERIC LONG RANGE AIRCRAFT CONFIGURATION

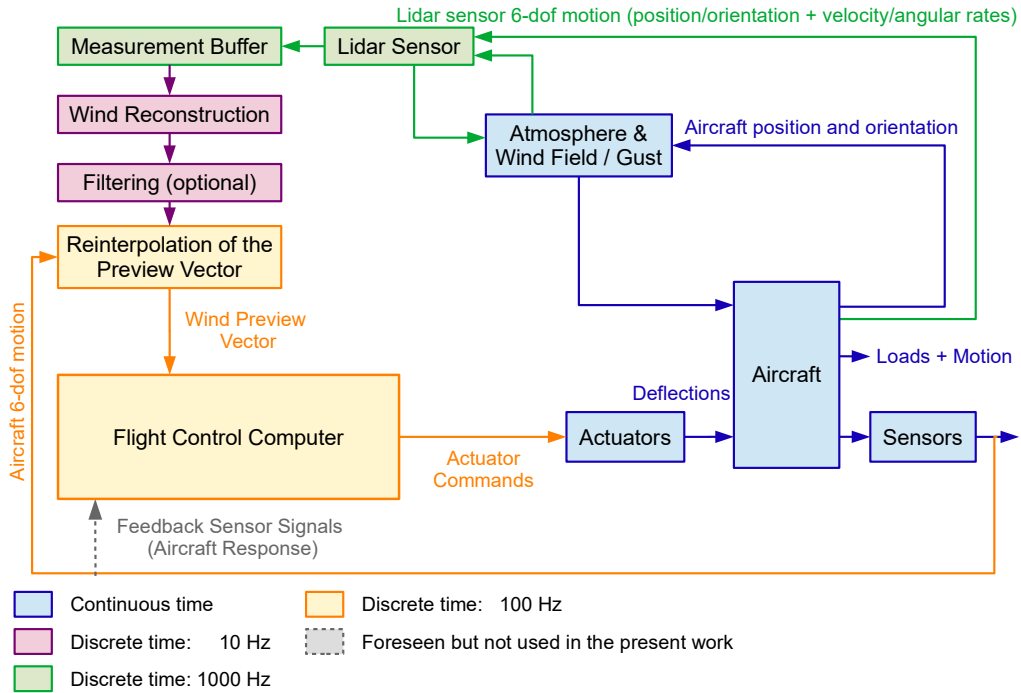


Figure 3: Overview of the Multi-Rate Hybrid Simulation of the Complete System

limits. These parameters can be adjusted: for each actuator independently, depending on the flight point, and asymmetrically (e.g. to account for the aerodynamic and inertial loads acting on the control surface). They are implemented as C++ S-functions.

Currently, only the actuators for the elevator and the ailerons are controlled by a control function. In the present work, all controlled actuators are adjusted via the same fixed (irrespective of the current flight point) parameters (low-pass cut-off frequency of 4.875 Hz, a damping coefficient of 0.9 and a gain of 1.0). Specific non-linear limitations for the control surface positions and rates are implemented additionally, specifically defined for each corresponding control device group, as can be seen (as actuator drive-train limitations) in the following table:

Table 2: Implemented Non-Linear Control Device Command and Actuator Limitations

Control Device Group	GLA-specific Command Limitations		Actuator Drivetrain Limitations	
	Deflection	Rate	Deflection	Rate
Elevators	$\pm 20^\circ$	$\pm 50^\circ/\text{s}$	$\pm 25^\circ$	$\pm 50^\circ/\text{s}$
Ailerons	$\pm 20^\circ$	$\pm 50^\circ/\text{s}$	$\pm 25^\circ$	$\pm 50^\circ/\text{s}$

The non-linear actuator drive-train limitations are the same for the entire flight envelope. Additionally, “GLA-specific Command Limitations” are implemented (see later in Figure 5). They restrict the gust load alleviation authority directly in the flight control computer. In the present work, only the feedforward preview GLA function is implemented, but if a feedback GLA function would be used as well, these limits would apply to the sum of their commands.

### 2.3 Considered Gust Load Cases

The simulated gust load cases are defined according to paragraph CS 25.341a [23]. To ensure a detailed evaluation of the preview-controlled aircraft behaviour in comparison to the open-loop aircraft behaviour, a representative set of gust load cases was chosen for analysis. The chosen set of gust load cases consists of symmetrical gusts with 20 different gust lengths. Symmetrical gusts are characterised by a constant wind velocity over the complete wingspan. The gust lengths are distributed equidistantly between 9 m and 107 m. All gust lengths are simulated twice as an upward and a downward gust separately. A total of 40 different gust load cases are simulated per linear model, leading to 2160 gust load cases per controller configuration. Hence, the analysis of the controller performance is based on exploiting symmetrical load cases (wings level, no sideslip, no lateral gust) solely. Therefore, it is assumed to be sufficient to illustrate only results for the right side of the aircraft (load stations of the right wing respectively of the right side of the horizontal tailplane) to discuss the structural behaviour in detail.

### 3. Controller Design Method

#### 3.1 Overall Workflow

The model described in section 2.1 enables to perform simulations to investigate the behaviour of a modern flexible aircraft during flight through atmospheric disturbances, especially in terms of the structural behaviour (the occurring loads) and the impact on general flight dynamics. However, creating models which are suitable to be used for numerous simulation purposes accompanies in the case of the GLRA with a complex model structure comprising nearly three thousand states and quite high-frequency modes (with significantly higher frequencies than those of interest for gust load alleviation). This model can be used (almost) directly for simulations/evaluations, but some modifications are necessary for the design of controller functions. These modifications, which also relate specifically to the design of a lidar-based load alleviation function, are described afterwards. These steps are also schematically represented in Figure 4. In the following, the explanations focus on specific steps and choices made for this specific application. For a broader overview on all involved processes and methods, the reader is referred to previous publications [5, 20].

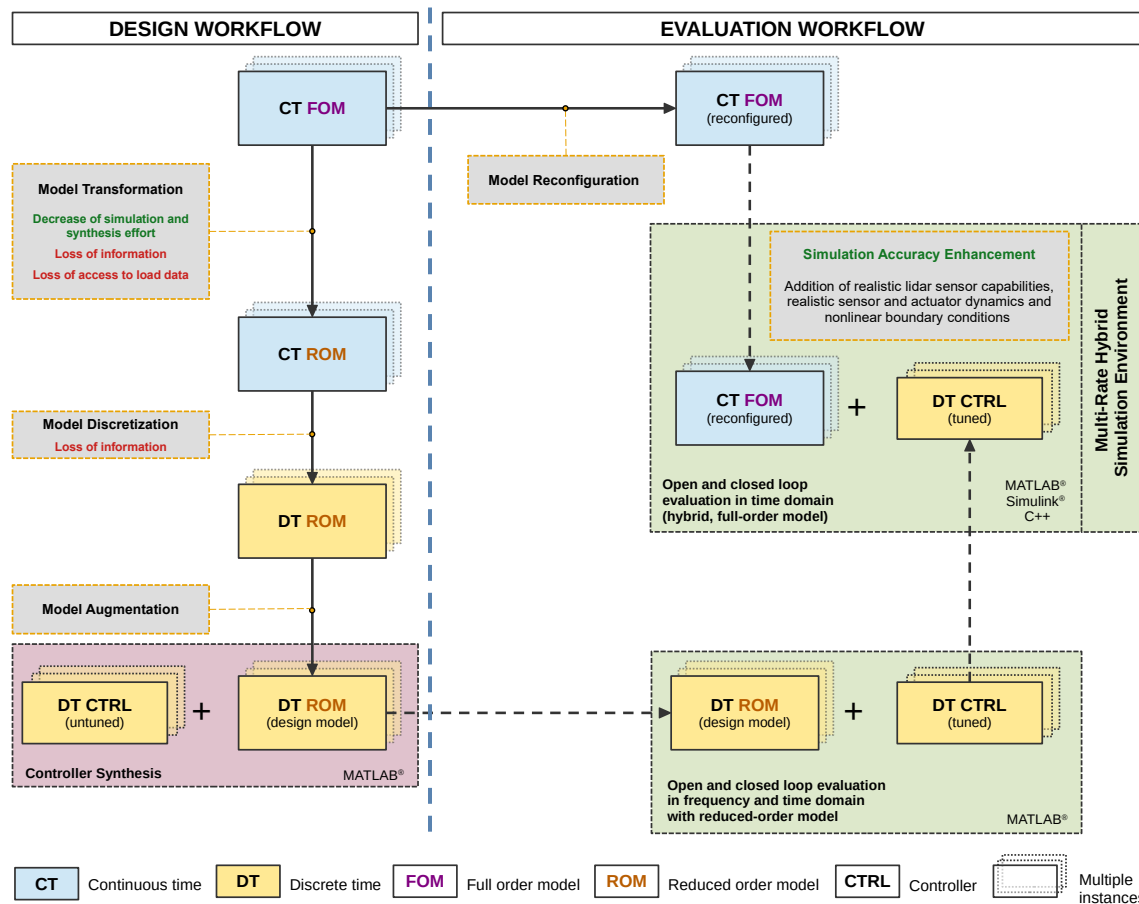


Figure 4: (Simplified) GLRA Data/Model Flow during the GLA Controller Design and Evaluation Process

The workflow used to develop the controller is designed for the use of modern, robust controller optimization methods. These optimization methods are provided by MATLAB<sup>®</sup> through the *sysune* function. The effort required to solve the considered control design problems increases with the complexity of the problem. A certain trade-off between size/representativeness of the design models used and usefulness of these models for controller design needs to be made. In addition to this trade-off further modifications/transformations are needed to obtain a model that can be used for discrete-time  $H_\infty$  or  $H_2$  control synthesis.

##### 3.1.1 Design Workflow

The process to modify the aeroelastic models is shown (in a simplified manner) on the left side in Figure 4. The original models are labelled CT FOM (Continuous Time Full Order Model(s)). Several augmentation and simplification steps yield the continuous-time reduced-order model (CT ROM).

## LIDAR-BASED GLA - RESULTS OBTAINED ON A GENERIC LONG RANGE AIRCRAFT CONFIGURATION

The original aeroelastic models are built with different zones with separate wind inputs for each zone and with separate inputs for wind/control surface deflections and their time-derivatives. They are transformed using Padé approximations [32] to account for time delays. Pseudo-differentiator filters (e.g.  $s/(\epsilon s + 1)$  with a small value for  $\epsilon$  compared to the inverse of the angular frequencies that need to be controlled) are used to replace groups of inputs which are time-derivatives of each other with a single equivalent input.

For a reduced computational effort and numerical robustness reasons, a model reduction process (consisting of numerous different model reduction steps) is required prior to the controller synthesis, transforming the modified full-order model into a reduced-order model (CT ROM). Prior to the model reduction, inputs and outputs which are unnecessary for the controller synthesis or the first simple evaluation steps are removed so that the model reduction process does not consider them when trying to match the behaviour of the full-order model as closely as possible. The transfers from gust input and control surface inputs to the considered load stations must be sufficiently accurate, especially within the frequency band of interest (typically 0.3 to about 8-10 Hz for active gust load alleviation). As pointed out in [5], pre- and postscaling of the different inputs and outputs are often required to obtain a well-balanced reduced model quality. It is also advisable to check each the match of the transfer functions defined by each input and output combination (cf. [5, Figures 2-4]). During the reduction a stronger focus was set to the inner part of the wing and slightly higher mismatch were tolerated towards the wing tip. Eventually, after several iterations on the model reduction parameters (scaling, order, etc.), the models were reduced from almost 3000 thousands to about 100 states. This order still permitted to reach a very good representativeness.

As already pointed out in [33, 34], the preview control approach used to design the lidar-based feedforward controller is easier to express as a discrete-time control synthesis problem. Thus, reduced discrete-time models (DT ROM) are generated by discretising the CT ROM models and later augmented by linear filter representing realistic lidar and wind reconstruction capabilities [19]. Finally, some of its transfers are normalised, and weighted to obtain a standard control synthesis problem [5, 20] on which the synthesis is made in discrete time.

### 3.1.2 Evaluation Workflow

While designing the gust load alleviation controller (process explained in the following sub-sections) and, eventually, for assessing the performance of the final controller, specific evaluation steps and environments are required as well (cf. right side of Figure 4).

The quickest and simplest validation option directly uses the designed controller with the (discrete) model it has been designed for (after removing some weighting functions used only for design), cf. lower right corner of the diagram in Figure 4. Evaluating the controllers with the design models is useful as the actual targets in terms of gust load alleviation, e.g. peak load in response to a one-minus-cosine gust, are not easy to formulate with frequency-domain criteria. So the evaluations made provide insights on the controller performance based on metrics that are not directly part of the *goal function* during the optimisation.

Performing time simulations with the most simple linear models is very fast compared to the evaluations which can be made with the multi-rate hybrid simulation environment presented in Figure 3. Frequency-domain analyses are also much faster than with the full-order models (a few seconds vs. several hours on a standard desktop computer). While using this linear models and as shown in [19, Fig. 15] for a different long range aircraft, it is crucial, for a sufficient accuracy of the evaluations made, to account for the lidar and wind reconstruction performance already at this stage.

If the load alleviation performance of the tuned (gain-scheduled) controller is deemed satisfactory, then it is worth performing a more precise evaluation of its performance using the heavier and more time consuming multi-rate hybrid simulation environment (upper right corner of Figure 4). The load alleviation results shown later in section 4 are all based on the multi-rate hybrid simulation.

## 3.2 Flight Control Functions

The gust load alleviation control concept demonstrated in the present work is a pure feedforward preview controller. The results presented hereafter show the achievable performance, when considered separately, and the way such controller can be tuned. In practice, the feedforward gust load alleviation controller would have to be combined with other control functions, such as baseline controllers (e.g. manual control laws, autopilot functions) and feedback gust load alleviation controllers. Figure 5 shows how these functions would be interconnected and some of the aspects that need to be considered for ensuring that feedback and feedforward control functions do not fight each other will be published in the near future. For instance, the pitching motion that the feedforward preview control function would typically command before encountering the gust, could be seen as a deviation of the desired state by the feedback control functions, but they should not counteract it. In the following, we focus only on the feedforward preview-control-based gust

load alleviation function.

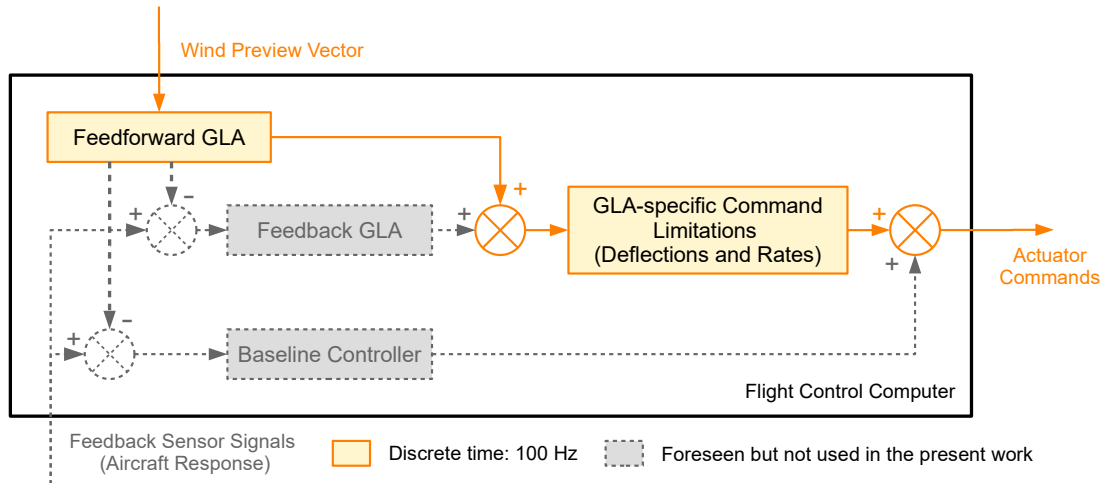


Figure 5: Considered Flight Control Functions and Their Interconnections

### 3.3 Feedforward Preview Controller Structure Used

To ease the tuning of the feedforward GLA controller, a structure with five multiple-inputs-single-output controllers working in parallel was defined. Each of these controllers commands a pair of control surfaces (e.g. left/right elevators, left/right inboard-most ailerons, etc.). Both surfaces receive the same command (i.e. only symmetrical commands are sent to the actuators). Imposing such a strong structure of the controller can lead to loss in achievable performance, but the results shown later indicate that the performance level reached is sufficient.

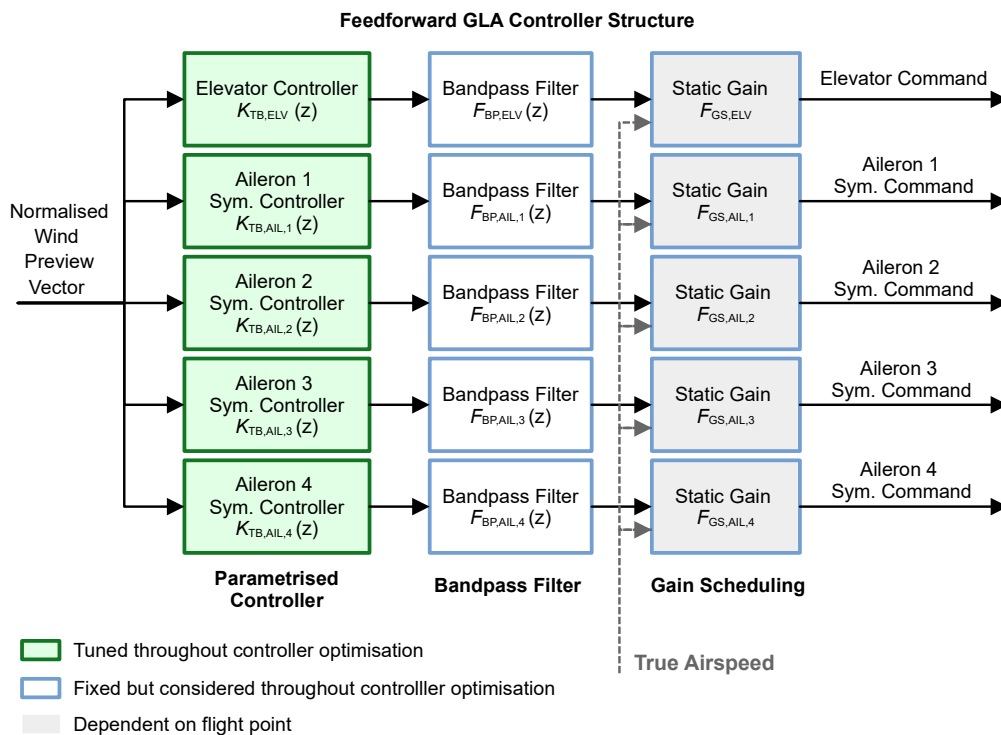


Figure 6: Internal Structure of the Lidar-Based Feedforward/Preview Controller

Each of the five parallel control “loops” consist of the same parts/steps. Each of these controllers consists of a parametrised (i.e. tunable), a fixed (bandpass filter), and a gain-scheduled part connected in series. All parts are directly or indirectly tuned by the user, but the “tunable” part is tuned by control synthesis algorithms, whereas the

## LIDAR-BASED GLA - RESULTS OBTAINED ON A GENERIC LONG RANGE AIRCRAFT CONFIGURATION

others are set/tuned manually. The following sections (3.3.1-3.3.4) describe each of these elements in the order of the control chain (i.e. going from left to right in the block-diagram of Figure 6).

### 3.3.1 Wind Preview Vector

The feedforward/preview controller expects to receive the estimated wind ahead of the aircraft as input. In classical/most formulations of preview control, the previewed signal is not a vector over time but simply a measured value for that signal taken in advance. The controller can “remember” the time evolution of this value to act at the right time and consider the evolution and trend over time thanks to its internal states. In this work, the preview signal is the estimated vertical wind ahead of the aircraft and the memorization of the successive estimates is done in the wind reconstruction module. The controller receives a wind profile as a vector of wind estimates (signal entering on the left side of Figure 6) along a portion of the flight path starting slightly behind the aft of the aircraft and ending at the position that the aircraft reference point will have in  $h_{\text{preview}}$  time steps (cf. Figure 7). This allows a clean separation between the required short-term memory of the the previewed signal and the frequency response of the controller. It also allows to improve the estimates for given position in space, as additional lidar measurements are received [6, 33–35].

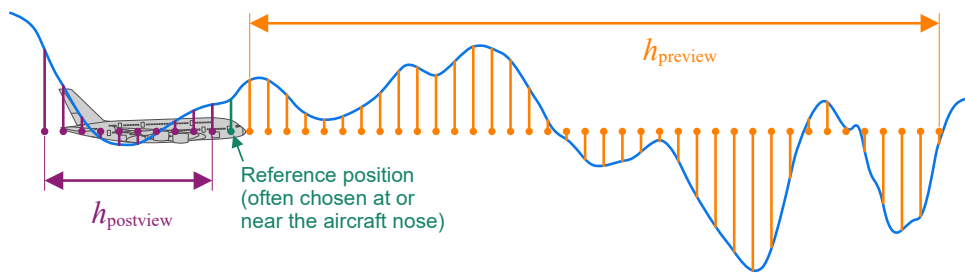


Figure 7: Preview and Postview Discretization of the Wind Field

Depending of the considered aircraft, the values  $h_{\text{postview}}$  and  $h_{\text{preview}}$  need to be adapted to the size of the aircraft, the critical gust lengths, and the chosen reference position. The farthest point also need to be compatible with the measurement range of the lidar. In practice, with geometrical effects and the need to have a minimum number of measurements performed around the farthest locations considered to obtain a sufficiently precise estimate of the vertical wind, the farthest point considered in the preview vector used by the controller is not as far as the farthest measurements performed by the lidar sensor. In the considered application, the farthest points measured by the lidar sensor were always (i.e. for all flight points) at about 182 m ahead of the aircraft nose, whereas the farthest point considered in the preview vector was only at about 148 m ahead of the aircraft nose. This corresponds to at least 0.560 s when flying at the maximum true airspeed value of 264.26 m/s of the considered flight points. As the controller is discretized with a sampling time of 10 ms, this corresponds to  $h_{\text{preview}} = 56$  samples. To ensure that the entire aircraft geometry, i.e. from the reference point around the nose position up to the tail, is covered by the preview vector,  $h_{\text{postview}}$  was set to 26 samples. The size of the wind vector in input of the controller block is then  $n_{\text{inputs}} = h_{\text{preview}} + 1 + h_{\text{postview}} = 83$ . This corresponds to the maximum available wind vector length that the different sub-parts of the controller could use. However, as it will be explained in section 3.3.2, some sub-parts of the controller are not using all wind information.

For easier interpretation of the controllers later on, the previewed vector is normalised by dividing the vertical wind velocities with the true airspeed.

### 3.3.2 Parametrised Controller

Each of five individual controllers that are working in parallel ( $K_{\text{TB,ELV}}(z)$ ,  $K_{\text{TB,AIL,1}}(z)$  to  $K_{\text{TB,AIL,4}}(z)$ ) receives the entire preview vector with 83 elements described above. However, the wind information at the tail of the aircraft is mostly useful for the pitching controller, as the wing already passed this location. So, for simplification of the tuning, the aileron controllers only receive the front most 73 out of 83 elements of the vector as the last 10 elements are located behind the main wing.

Each of these five controllers could, in principle, be a fairly complex parametrised discrete-time controller. In this work, the controllers were simply a static gain matrix (i.e. a  $1 \times 83$  matrix for the elevator controller and  $1 \times 73$  matrix for each of the aileron controllers). This leads to a total of  $83 + 4 \cdot 73 = 375$  tunable parameters. Even if the parametrised part of the controller is here defined as a static gain matrix, the transfer function from the vertical wind/gust to the output of the controller should be seen as a finite impulse response (FIR) filter: the previewed wind vector can be seen as a tapped delay line and the gain matrix as the FIR filter gains (cf. [19, 36]).

## LIDAR-BASED GLA - RESULTS OBTAINED ON A GENERIC LONG RANGE AIRCRAFT CONFIGURATION

The tuning and the number of preview and postview elements were defined based on the most critical flight points, which are also the flight point with the highest true airspeed in this case. For lower speeds, it could make sense to increase the number of preview and postview elements. As shown above, the number of preview elements is defined based on an effective measurement range and the number of time steps needed to cover this distance. At lower speeds, it would potentially take more time steps to cover the same distance and hence  $h_{\text{preview}}$  could be increased. Similarly, the number of time steps needed for the tail of the aircraft to reach the current position of the chosen reference position also becomes larger. For simplicity, the number of preview and postview elements were kept constant, which means that they are slightly suboptimal for lower speeds. As the loads levels were lower at these lower speeds, the loss of optimality for these flight points is not impeding the overall reached gust load alleviation performance in terms of load envelope (see results presented later).

### 3.3.3 Bandpass Filters

In addition to the tunable part of the controllers, band-pass filters  $F_{\text{BP,ELV}}(z)$  and  $F_{\text{BP,AIL},1}(z)$  to  $F_{\text{BP,AIL},4}(z)$  are defined by the designer and connected in series with the different controllers. In the first step of the tuning, these filters were identical and obtained by discretising the following Laplace transfer function (with Tustin's method).

$$F_{\text{BP}}(s) = \overbrace{\frac{s}{(2 \cdot \pi \cdot 0.05) + s}}^{\text{high-pass filter}} \cdot \underbrace{\frac{1}{\frac{1}{2\pi \cdot 5.00} \cdot s + 1}}_{\text{low-pass filter}} \cdot \underbrace{\frac{1}{\frac{1}{2\pi \cdot 7.00} \cdot s + 1}}_{\text{low-pass filter}} \quad (1)$$

The filter is defined in continuous-time because the numerical values of the transfer function coefficients are easier to interpret for the control designer than it would be the case with discrete-time transfer functions. These filters are part of the tunable plant used during the control synthesis: the tunable part of the controller can therefore account for them, even if it is not allowed to tune them.

The band-pass filter cuts the lowest frequencies (i.e. below 0.05 Hz) as well as the highest frequencies (i.e. above 5–7 Hz). Cutting the lowest frequencies ensures that no constant or quasi-constant deflections can be commanded, which is desirable. In the pitch axis, such constant deflection would interact with the aircraft trim and the flight mechanics. On the ailerons, this would impact the flight shape of the wing and the flight performance. Cutting the highest frequencies prevents from propagating measurements noise to the control surfaces, especially at frequencies (i.e. gust scales) that are not well measured by the lidar [6].

### 3.3.4 Gain Scheduling

The most critical flight points are the ones at higher speeds. Assuming that a controller was tuned for the critical point, to figure out which gain scheduling strategy should be followed, one should answer the following question: “What should be modified in the controller behaviour to adapt the controller to a different flight point?”

Putting aside drastic changes with Mach number especially in the transonic regime, the following simplified dependencies with the airspeed can be found. The aerodynamic forces, and in particular the lift on the wing, increase quadratically with the true airspeed, as the dynamic pressure does. So for an identical change in angle-of-attack, the increment in lift caused by this changes also scales quadratically with the airspeed (i.e.  $V^2$ ). At the same time, gust itself should rather be seen as a vertical wind change and not a change in angle-of-attack. For a constant change in vertical wind, the corresponding change in angle-of-attack scale with the inverse of the true airspeed (i.e.  $1/V$ ). Eventually, the combination of the two, leads to a change in lift increment that scales linearly with the airspeed ( $V^2/V = V$ ). This dependency has been known for many decades and is also used in the well-known  $V - n$  diagrams.

This said, the local lift increment due to an aileron command also scales quadratically with the true airspeed (assuming no speed/Mach-induced loss of effectiveness of the control surface). And so, for matching a gust-induced lift increment that scales linearly with a control surface whose effectiveness scales quadratically with the true airspeed, one could expect to reduce the control gain with increasing true airspeed (respectively increasing the control gain with decreasing true airspeed). But, the load and aeroelastic behaviour is slightly more complex and the goal of the gust load alleviation controller is not to reach the same relative level of load alleviation performance at all flight points! Instead, its goal is to shrink the gust load envelope: an equally large relative improvement for flight points that are not sizing as for those which are sizing is not needed. For instance, if the goal is to shrink the peak load envelope by 20 percent overall, the peak load levels for a flight point that is only at 90 percent of the worst case in open-loop only need to be reduced by 12.2% ( $0.888 \cdot 0.9 \approx 0.8$ ).

Another aspect to consider for the gain scheduling, is that when computing the gust load envelope, the amplitudes of the gusts defined in paragraph CS 25.341a (cf. [23]) not only depend on the gust length but also of some aircraft

## LIDAR-BASED GLA - RESULTS OBTAINED ON A GENERIC LONG RANGE AIRCRAFT CONFIGURATION

parameters and of the flight point. When considering the gain-scheduling for a specific aircraft, the aircraft parameters are fixed. However, the dependency on the flight point still needs to be considered. The formulas are not very simple and partly defined with piecewise functions of the altitude, expressed in equivalent airspeed, and so this involves also a conversion to true airspeed. The details computations are not too important here and can be found in [23]. The important point here is that the gust amplitude to be considered, expressed as true airspeed, does increase with the true airspeed but less than the true airspeed itself.

In the end, the controller receives normalised vertical wind components (i.e. similar to a gust-induced angle-of-attach increase, when a small angle approximation can be made) and the controller outputs are scaled with the true airspeed, as indicated in the following formula:

$$F_{GS,ELV}(s) = F_{GS,AIL,1}(s) = F_{GS,AIL,2}(s) = F_{GS,AIL,3}(s) = F_{GS,AIL,4}(s) = \frac{V_{TAS,FP}}{V_{TAS,ref}}. \quad (2)$$

This leads to a lower relative load alleviation for the non-critical flight points (lower speeds than the worst case). This prevents unnecessarily large alleviation levels at these flight points.

### 3.4 Multi-Model Iterative Tuning of the Controller

The tuning of the lidar-based gust load alleviation function is almost never done in a single pass, but rather an iterative process in which the *control synthesis* is only a step. There are two main reasons for this. First, it is not always possible to define the correct values for all *weighing functions* or *templates* beforehand. Whilst the reduction of the gust response to a certain level can be fairly well specified on its own, the trade-off between different load types and stations across the airframe in combination with the control surface activity, often requires the designer to weigh different options, analyse them in simulation (potentially with various levels of representativeness of the simulation environment used), and loop back with slightly adjusted specifications. For conciseness reasons, this iterative process is not detailed further, but the interested reader can refer to the process shown in [5, Fig. 1], as it corresponds to the process used also in the present work. Compared to the work shown in [5], the iterative process was made easier by combining it with the linear filter approximation of the lidar-based wind estimation losses proposed in [19].

In the present controller design, reducing the bending moment at the wing root was the top priority. For this reason, a template (transfer function) was defined to optimise the transmission behaviour between the wind input and the bending moment output at the wing root. Based on the analysis of the open-loop gust load envelope four models were initially selected. They correspond to the mass cases with the highest total mass (MZmMe, MTFFJ, MTAAJ, MTmMG) at the highest true airspeed and the *clean-wing* configuration. These models were generating the sizing gust loads for the wing. No *airbrake-out* cases were considered at this stage, even they are sizing for the outer part of the wing (see results later in Figure 9), because these models were not available yet.

Whilst reducing the bending moment at the wing root was the top priority, large loads increases at other locations or excessively large and fast control surface commands should be prevented. For this, further criteria were added during the tuning. The limits on the control surface deflections were defined in such a way that the specifications regarding control surface deflections or rates are not to be expected to be exceeded in the subsequent evaluations with the certification gusts.

The initial tuning was performed with the four *clean wing* models selected and with 6 different criteria, so 24 performance channels in total. A good trade-off between the different control objectives was rapidly obtained. The controller made good use of the available authority on the ailerons and elevators to obtain a very significant loads reduction, while not being exaggeratedly aggressive. After finishing the first iterative tuning, the *airbrake-out* cases became available and further analyses were performed including these cases as well. It was found that the designed controller performed very well also on the *airbrake-out* cases for all mass cases and flight points.

Upon further analyses, it was found that the pitching behaviour was potentially very slightly more aggressive than necessary and just reached the elevator rate limiters in the extreme-most cases<sup>2</sup>. Instead of re-looping-back with slightly different specifications and re-tuning the entire controller, the gain of the band-pass filter for the elevator command was simply reduced by 10% (i.e. by setting  $F_{BP,ELV}(s) = 0.9 \cdot F_{BP}(s)$ ).

<sup>2</sup>Note that the certification cases are defined to be extreme conditions: in most conditions and flights through turbulence, the encountered gusts are significantly smaller and so would the controller commands as well. Reaching the rate or position limits would not have catastrophic consequences either: the designed controller architecture is for instance not subject to winding of integrators nor would specific behaviours be triggered by that.

## 4. Results

This section presents current results for the Generic Long Range Aircraft (GLRA) model with the controller tuned using the set of tools presented in the previous section. To simplify future references and comparisons, e.g. in future publications, this particular feedforward controller is called **DLR-FT-GLRA-GLA-FF-v1** from now on. For the evaluation, 2160 gust load simulations (combinations of the 54 linear models, 20 gust lengths, 2 gust directions) are performed to determine the load envelope for all considered configurations. Two configurations are considered: *open loop* and with the presented feedforward preview control being active (referred simply as *preview controller* in the following). To ensure a sufficiently fine evaluation “grid” for the structural loads, 40 loads stations were selected on each wing as well as 19 stations for each half of the horizontal tailplane. At each of these load stations, all six cut loads (bending moment, torsional moment, in-plane bending moment, vertical shear force, longitudinal shear force, lateral force) are considered. A representative selection for the most relevant load stations and types are shown hereafter.

### 4.1 Quantitative Evaluation of the Controller Behaviour

#### 4.1.1 Gust Load Envelope

Figure 8 shows the respective gust loads envelopes obtained based on the 2160 gust encounter simulations with the feedforward preview controller active compared to the 2160 ones in open loop.

The feedforward preview controller achieves a quite significant reduction of the peak bending moments along the wing: about 17–18 % around wing root (important location for wing weight), close to 20 % load alleviation around one third of the wing span, and then reducing to about 10–12 % improvement near the wing tip.

The impact on the peak torsional moments is slightly more complicated. First, it should be noted that the highest torsional moments are in the negative direction, so the relative improvement figures shown considers the peak negative torsional values in both cases: in open-loop and with the preview controller. Between the ailerons and the engine, an increase of the peak torsional moment by 2–4 % seems not avoidable, at least when aiming for large bending moment reductions. At wing root and in the last third of the wing span, the torsional moment is reduced by 5–10 %.

In addition to the in-depth view on the structural behaviour of the wing structure, the bottom plots in Figure 8 shows the peak bending and torsional loads envelope for the horizontal tailplane. The pitching manoeuvres which permits to reduce the lift increase on the wing yields significant increases in both the bending and the torsional moment on the horizontal tailplane. No values are available for other types of load cases (e.g. manoeuvre loads) for this aircraft configuration. However, it can be assumed that the loads generated by the preview controller will be smaller than, for example, the manoeuvre-related loads required by the certification rules (cf. comparatively small vertical load factor values reached during the anticipated reaction to the forthcoming gusts in Figures 10-13, introduced later in section 4.2). The certification rules call for pitching manoeuvres up to a vertical load factor of 2.5 g (upwards) and –1 g (downwards), which is well beyond the typical range of  $1 \pm 0.5$  g that the pitching controller commands on these extreme gust cases.

#### 4.1.2 Clean-Wing vs. Airbrake-Out Loads Envelopes

The consideration of *airbrake-out* cases is rarely made in the literature, even if these cases are most likely considered during new aircraft development and certification. Indeed, fairly high-speed descents with airbrakes are flown relatively often, for instance when pilots try to catch up some delays. When encountering a gust with extended airbrakes, the lift distribution, flight shape, and the gust-induced local lift forces and pitching moments change. The spoilers are already deflected such that a no additional lift reduction can be obtained by deflecting the spoilers.

Figure 9 presents the gust envelopes as previously shown in Figure 9, but with an additional decomposition in *clean-wing* and *airbrake-out* envelopes. For each case (*open loop* and *preview controller*) the maximum values obtained on both sets of load cases (i.e. *clean-wing* and *airbrake-out*) corresponds to the envelope shown in Figure 9. The *open-loop* envelope (i.e. with both sets of load cases) is used for normalisation. As for Figure 9, the minimum values for the torsional moment along the wing span are shown because they are larger, in absolute value, than the maximum ones.

Depending on the type of load (here bending vs. torsional moments) and the location along the wing, the peak loads that are defining the envelopes, as shown in Figure 8, are partly obtained with the *clean-wing* cases and partly with the *airbrake-out* cases. For the *preview controller* configuration, the *airbrake-out* cases yield lower bending moment loads for all but one station along the wing, whereas these cases were the dominant ones for the entire outer half of the wing in *open loop*. The relative loads levels for the torsional moment remain almost the same for both configurations (i.e. *clean-wing* vs. *airbrake-out* both in *open loop* and *preview controller* cases). It remains to be investigated whether this behaviour (both for bending and torsional moments) is specific to the considered long range

## LIDAR-BASED GLA - RESULTS OBTAINED ON A GENERIC LONG RANGE AIRCRAFT CONFIGURATION

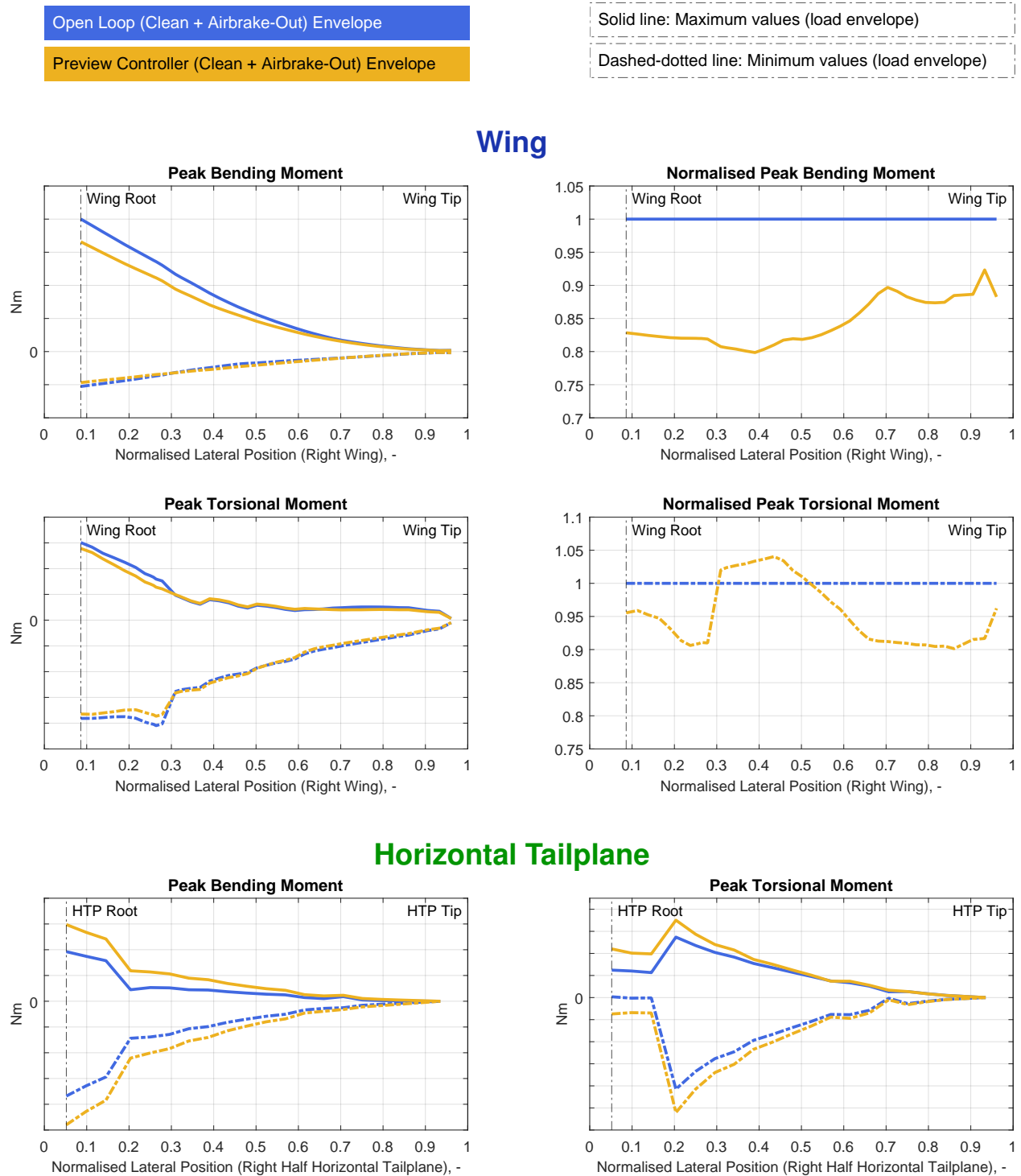


Figure 8: Gust load envelopes for right wing and right HTP, computed with the multi-rate hybrid simulation environment using the continuous-time full-order models (CT-FOM): open loop vs. with preview controller.

aircraft and/or the specific preview controller tuning performed, or whether such trends should be expected for other similar aircraft configurations as well.

## LIDAR-BASED GLA - RESULTS OBTAINED ON A GENERIC LONG RANGE AIRCRAFT CONFIGURATION

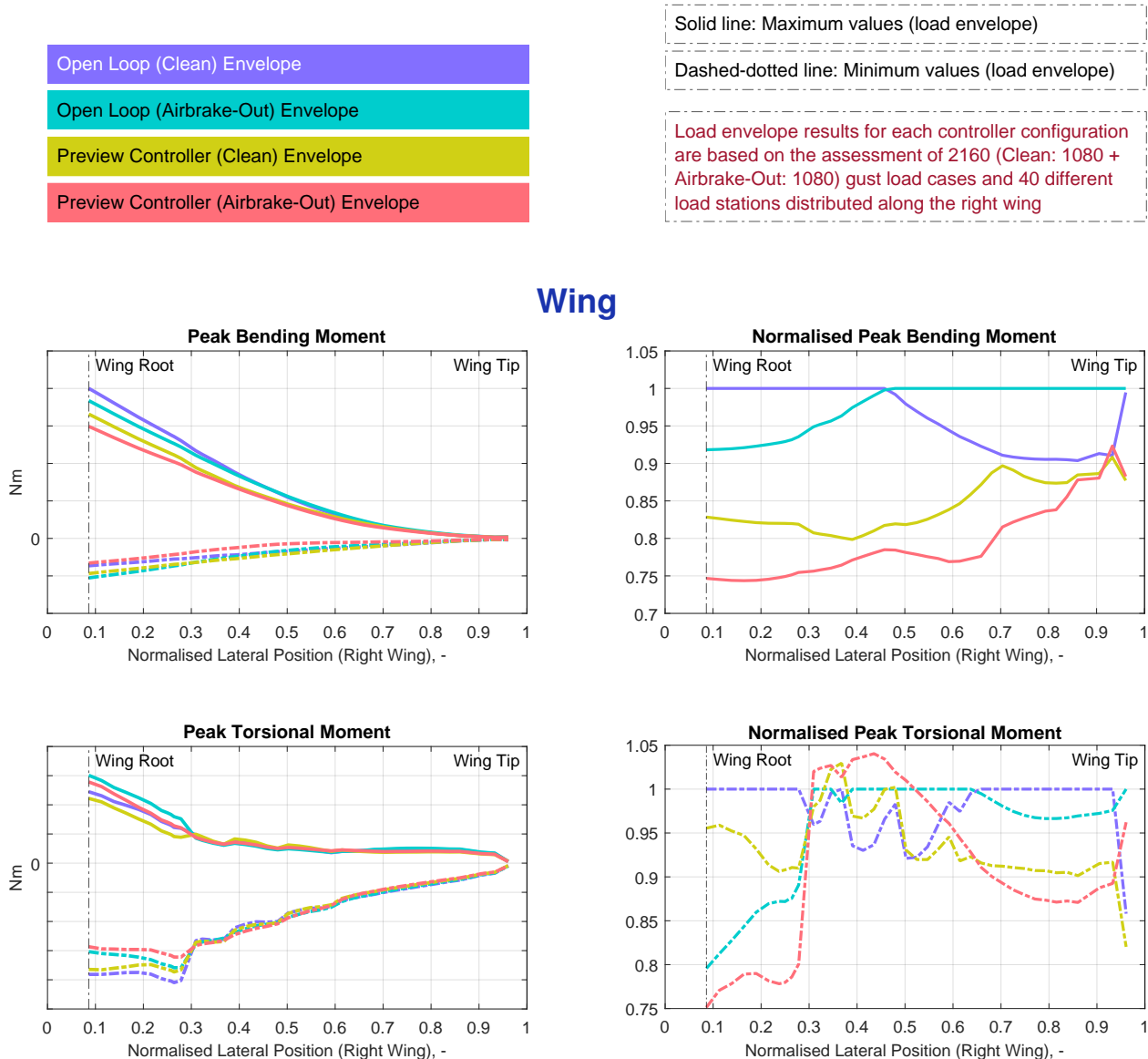


Figure 9: Gust load envelopes for the wing, as in Figure 8, but separating the *clean-wing* and *airbrake-out* cases.

#### 4.2 Qualitative Evaluation of the Controller Behaviour

Apart from the *quantitative* results shown in the previous section with the performance in terms of load envelope reduction, it is useful to analyse the controller strategy by looking at time series plots. It also permits to detect any potentially surprising behaviour (e.g. inboard and outboard ailerons with opposite deflections in an attempt to control higher frequency modes of the wing).

To ease this detailed analysis for all flight points and gust cases, standard overview plots specific to the GLRA configuration are generated for every gust load case (one for each combination of mass case, flight point, gust length and direction). Logically, only a small selection of these plots are shown here (Figures 10-13). The selected cases are representative of the overall range of behaviours obtained. For better comparability only *clean-wing* cases are shown, but the qualitative behaviour is similar on the *airbrake-out* cases. Also for comparability only one flight point is included:  $H = 8300\text{ m}$ ,  $V_{TAS} = 264.26\text{ m/s}$ . The cases shown are combinations of two of the most challenging mass cases (MTmMG and MTFFJ) and a few gust lengths (always upward gusts).

Figures 10-13 are structured as follows. At the top, all relevant parameters to define the load cases are shown, i.e. the model, mass cases, flight point, gust parameters, etc. as well as the gust profile over time. Just below, the control surface deflections and deflection rates are shown. The ailerons 1 and 2 are grouped in the middle plot and the ailerons 3 and 4 grouped in the right plot. The lower half of the each figure consists of 12 plots arranged in a  $4 \times 3$  matrix.

## LIDAR-BASED GLA - RESULTS OBTAINED ON A GENERIC LONG RANGE AIRCRAFT CONFIGURATION

The left column of this matrix contains *rigid-body* parameters, whereas the other two columns show 8 different loads out of over 2500 load outputs available for GLRA aircraft model. The selected loads shown in the second column are the bending moment at wing root, about one-third of the wing span, two-third of the wing span, and the root of the horizontal tailplane. The third column shows the torsional moment for the same stations than in the second column.

The blue lines correspond to the open loop aircraft behaviour and the other lines corresponds to the aircraft controlled by the lidar-based preview control gust load alleviation function. The considered aircraft has four ailerons per wing, the inboard-most two ailerons and the outboard-most two ailerons are represented on different plots and within each of these plots a plain line is used for the inboard-most one of the two and a dashed line for the other.

In all plots related to aircraft excitation, it can be seen that the controller makes reasonable use of the allowed authority (both in position and rates) over commanded control surface deflections, especially considering that these are extreme gust cases. The authority used decreases with decreasing gust length. The maximum deflections are fairly far from the overall limits, but the control surface rates are closer to the limits. Still this shows that it would be possible to tune a more aggressive gust load alleviation controller, but that is not necessarily desirable. The level of load alleviation reached shall permit to make the gust load cases not sizing as lower than other cases.

As expected with a lidar-based gust load alleviation controller, the pitching commands (elevator commands) are starting prior to the time of the gust impact, such that a minor variation of the angle of attack respectively a significant unloading of the wing prior to flying into the gust happens. This precompensation of the angle of attack is very effective in reducing the wing root bending loads that occur over time. In addition, such an unloading in advance is not necessarily be problematic and should not be uncomfortable for the passengers (compare plots for the vertical load factor).

The deflections of the three inboard-most ailerons are almost identical. The outboard-most aileron is very slightly delayed/phase-shifted and deflected with a lower amplitude. The motion of the ailerons seems to partly compensate for the pitching movement caused by deflecting the elevator. During the pitch-down motion which is commanded in anticipation of the forthcoming upward gust, the ailerons are deflected in the positive direction (i.e. trailing edge downwards), which mitigate the unloading of the wing due to the pitching motion. When the gust hits the wing, the ailerons are deflected upwards so that lift is reduced and the additional lift generated by the gust is partly compensated. This lateral shift in lift leads to an additional twisting of the wing, which, however, does not generate any additional maximum values for the torsional moments at the wing root. However, deflection of the elevator leads to a longitudinal shift of lift before and during gust passage towards the horizontal tailplane, which leads to additional bending and torsional moments at the root of the HTP (as seen in the *quantitative* evaluation in section 4.1).

Figures 10-13 are sorted in descending order of the considered gust lengths. The reduction of controller activity with decreasing gust length is moderate for the longer gust lengths but significant for the shorter ones. This results from two effects. First, the lidar sensor and wind reconstruction are not sensing the shorter gusts well. Second, the controller is tuned in the frequency domain and the focus is set on the sizing cases which are in the range of the longest gusts specified in the CS 25.341a [23]. So, both the tuning criteria selected by the designer and the band-pass filters used prevent the controller from being very active at higher frequencies (typically 5–7 Hz and above).

## 5. Conclusions

The design of a lidar-based load alleviation function for a long range aircraft configuration was presented. The controller was scheduled with the airspeed to account for the change in behaviour of the dynamic model as well as the fact that all flight points are not equally critical in terms of gust loads. The complete lidar-based load alleviation system was evaluated (including a very detailed lidar sensor model and the related post-processing algorithms) using a multi-rate hybrid simulation environment with the load alleviation controller running at 100 Hz. During the tuning phase and to increase the productivity of the control designer, significantly faster evaluations were performed with a simplified simulation environment.

It was possible to very finely tune the behaviour of the controller to obtain the desired load alleviation performance, even if there were slight differences between the results with this simplified environment compared to those of the hybrid multi-rate simulation (reference). This was expected, as the hybrid simulation contains a complete simulation of the lidar sensor, the acquisition system and post-processing/wind estimation algorithm whereas the design model contains a simplified linear approximation of the entire sensor chain. The lidar sensor and the regularised wind estimation roughly behaves as a low-pass filter, cf. [6], and so some frequencies are attenuated and others not detected/seen at all. Compared to the similar tuning that the authors performed on a different aircraft in [5] without using this linear approximation filter, the smaller mismatch between the design models used in this work (which included this filter) and the behaviour of the multi-rate simulation<sup>3</sup> made the tuning significantly easier for the designer. Recently, new

<sup>3</sup>Smaller mismatch on the wind input side, so for all transfers from the wind input to any of the outputs of the system.

## LIDAR-BASED GLA - RESULTS OBTAINED ON A GENERIC LONG RANGE AIRCRAFT CONFIGURATION

filters permitting to precisely focus on specific gust lengths and on a frequency-based performance metrics which more closely matches the peak response in the time domain to a 1-minus-cosine gust were proposed [36]. These filters were not used in the present work, but it is reasonable to assume that using these filters could ease the control design process even more.

The feedforward preview controller achieves a quite significant reduction of the peak bending moments along the wing: about 17–18 % around wing root (important location for wing weight), close to 20 % load alleviation around one third of the wing span, and then reducing to about 10–12 % improvement near the wing tip. It also balances the need for strong load reduction on the wing with the desire to have gentle control commands, avoiding too extreme loads redistribution (i.e. to other locations in the structure or other load types). This is made possible by the anticipation capability offered by the lidar sensor and makes such sensor concepts so promising.

The controller yields slight torsional load increase in the middle of the wing. Without structure resizing study similar to the one shown in [37, section 3.3.4], it cannot be said whether the moderate increase in peak torsional moment outboard of the engine would cause any significant weight penalty. It seems likely that the weight reductions that would result from the bending moment reduction would largely exceed the potential weight penalty, if any, caused by this slight increase in peak torsional moment. The load increases at the horizontal tailplane are likely to be significantly smaller than the manoeuvre loads (not considered in the present work) and therefore not causing any weight penalty.

The large load alleviation potential offered by using a lidar for gust load alleviation is not new and was also mentioned several times in the literature [3, 16] including by the authors, cf. for instance [5] where a similar preview control concept was demonstrated for a different aircraft configuration with much shorter critical gust lengths. Even if the preview control concept presented and evaluated in this work showed very promising performance levels, it would make sense to complement this purely feedforward gust load alleviation architecture with a feedback part as well. This is foreseen, as indicated in Figure 5, and is left for future work.

## 6. Acknowledgments

This work was performed and funded within the framework of the German national research project InFlyTec (Förderkennzeichen 20A1705C) and within the framework of the German national research project INTELWI (Förderkennzeichen 20A1903A), partly on the basis of prior work within the German national research project Con.Move and the Clean Sky 2 MANTA project. The authors thankfully acknowledge the funding received from the Federal Ministry for Economic Affairs and Energy (BMWi) and the Federal Ministry for Economic Affairs and Climate Action (BMWK).

The authors warmly thank the partners involved in these projects for the fruitful collaboration and for the continuous technical exchanges as well as various DLR colleagues who contributed to this work. Simon Binder, Özge Süelözgen, and Thiemo Kier from the DLR Institute of System Dynamics and Control, Vega Handojo from the DLR Institute of Aeroelasticity, and Patrick Vrancken from the DLR Institute of Atmospheric Physics contributed through the structural layout, the generation of the integrated aeroelastic model of the aircraft, the computation of load envelopes and the supply of a vital part of the lidar model. Davide Cavaliere and Daniel Kiehn, who are members of the authors' research group, contributed to this work through their respective work on the internal control design tool ALOA (Active LOad Alleviation) used in this work and the lidar and wind reconstruction algorithm, as well as through numerous discussions.

## References

- [1] J. H. Wykes. Structural dynamic stability augmentation and gust alleviation of flexible aircraft. In *AIAA 5<sup>th</sup> Annual Meeting and Technical Display*, Philadelphia, PA, USA, Oct., 1968. DOI: [10.2514/6.1968-1067](https://doi.org/10.2514/6.1968-1067).
- [2] E. Livne. Future of airplane aeroelasticity. *Journal of Aircraft*, 46(6):1066–1092, 2003. DOI: [10.2514/2.7218](https://doi.org/10.2514/2.7218).
- [3] G. Jenaro Rabadan, N. P. Schmitt, T. Pistner, and W. Rehm. Airborne lidar for automatic feedforward control of turbulent in-flight phenomena. *Journal of Aircraft*, 47(2):392–403, 2010. DOI: [10.2514/1.44950](https://doi.org/10.2514/1.44950).
- [4] N. Fezans, H.-D. Joos, and C. Deiler. Gust load alleviation for a long-range aircraft with and without anticipation. *CEAS Aeronautical Journal*, 10:1033–1057, 2019. DOI: [10.1007/s13272-019-00362-9](https://doi.org/10.1007/s13272-019-00362-9).
- [5] N. Fezans, C. Wallace, D. Kiehn, D. Cavaliere, and P. Vrancken. Lidar-based gust load alleviation - results obtained on the Clean Sky 2 Load Alleviation Benchmark. In *International Forum on Aeroelasticity and Structural Dynamics (IFASD)*, Madrid, Spain, Jun. 13–17, 2022. IFASD-2022-155. <https://elib.dlr.de/187462/>.

## LIDAR-BASED GLA - RESULTS OBTAINED ON A GENERIC LONG RANGE AIRCRAFT CONFIGURATION

- [6] D. Kiehn, N. Fezans, P. Vrancken, and C. Deiler. Parameter analysis of a doppler lidar sensor for gust detection and load alleviation. In *International Forum on Aeroelasticity and Structural Dynamics (IFASD)*, Madrid, Spain, Jun. 13–17, 2022. IFASD-2022-105. <https://elib.dlr.de/187627/>.
- [7] Y. Hamada, R. Kikuchi, and H. Inokuchi. Lidar-based gust alleviation control system: Obtained results and flight demonstration plan. *IFAC-PapersOnLine*, 53(2):14839–14844, 2020. ISSN: 2405-8963. 21st IFAC World Congress. DOI: [10.1016/j.ifacol.2020.12.1928](https://doi.org/10.1016/j.ifacol.2020.12.1928).
- [8] H. Inokuchi and T. Akiyama. Performance evaluation of an airborne coherent doppler lidar and investigation of its practical application. *Transactions of the Japan Society for Aeronautical and Space Sciences*, 65(2):47–55, 2022. DOI: [10.2322/tjsass.65.47](https://doi.org/10.2322/tjsass.65.47).
- [9] Á. Hannesdóttir, A. Meseguer Urbán, F. Spasov, and A. Larvol. Optimum gust detection by nacelle-based lidar: A study on the vestas v52. *Journal of Physics: Conference Series*, 2265(2):022072, May 2022. DOI: [10.1088/1742-6596/2265/2/022072](https://doi.org/10.1088/1742-6596/2265/2/022072).
- [10] D. Schlipf, E. Bossanyi, C. E. Carcangiu, T. Fischer, T. Maul, and M. Rossetti. Lidar assisted collective pitch control. Technical report, University of Stuttgart. EU FP6 UpWind Project Report - D5.1.3. [https://elib.uni-stuttgart.de/bitstream/11682/3930/1/D.5.1.3.\\_LIDAR\\_assisted\\_collective\\_pitch\\_control.pdf](https://elib.uni-stuttgart.de/bitstream/11682/3930/1/D.5.1.3._LIDAR_assisted_collective_pitch_control.pdf).
- [11] David Schlipf, Paul Fleming, Florian Haizmann, Andrew Scholbrock, Martin Hofsäß, Alan Wright, and Po Wen Cheng. Field testing of feedforward collective pitch control on the cart2 using a nacelle-based lidar scanner. *Journal of Physics: Conference Series*, 555(1):012090, dec 2014. DOI: [10.1088/1742-6596/555/1/012090](https://doi.org/10.1088/1742-6596/555/1/012090).
- [12] A. Meseguer Urban and M. H. Hansen. Lidar correlation to extreme flapwise moment : Gust impact prediction time and feedforward control. Technical report, 2017. <https://orbit.dtu.dk/en/publications/lidar-correlation-to-extreme-flapwise-moment-gust-impact-predicti>.
- [13] H.-G. Giessler, M. Kopf, P. Varutti, T. Faulwasser, and R. Findeisen. Model predictive control for gust load alleviation. *IFAC Proceedings Volumes*, 45(17):27–32, 2012. ISSN: 14746670. DOI: [10.3182/20120823-5-NL-3013.00049](https://doi.org/10.3182/20120823-5-NL-3013.00049).
- [14] B. Barzgaran, J. D. Quenzer, M. Mesbahi, K. A. Morgansen, and E. Livne. *Real-time Model Predictive Control for Gust Load Alleviation on an Aeroelastic Wind Tunnel Test Article*. DOI: [10.2514/6.2021-0500](https://doi.org/10.2514/6.2021-0500).
- [15] K.-Y. Ting, M. Mesbahi, E. Livne, and K. A. Morgansen. *Wind Tunnel Study of Preview  $H_2$  and  $H_\infty$  Control for Gust Load Alleviation for Flexible Aircraft*. DOI: [10.2514/6.2022-2489](https://doi.org/10.2514/6.2022-2489).
- [16] H. Fournier, P. Massioni, M. Tu Pham, L. Bako, R. Vernay, and M. Colombo. Robust Gust Load Alleviation of Flexible Aircraft Equipped with Lidar. *Journal of Guidance, Control, and Dynamics*, 45(1):58–72, 2022. DOI: [10.2514/1.G006084](https://doi.org/10.2514/1.G006084).
- [17] N. Fezans, P. Vrancken, P. Linsmayer, C. Wallace, and C. Deiler. Designing and maturing doppler lidar sensors for gust load alleviation: Progress made since AWIATOR. In *Proceedings of the Aerospace Europe Conference*, Bordeaux, France, Feb. 25–28, 2020. CEAS / 3AF. <https://elib.dlr.de/134227>.
- [18] N. Fezans, J. Schwithal, and D. Fischenberg. In-flight remote sensing and identification of gust, turbulence, and wake vortices using a Doppler LIDAR. *CEAS Aeronautical Journal*, 8(2):313–333, 2017. DOI: [10.1007/s13272-017-0240-9](https://doi.org/10.1007/s13272-017-0240-9).
- [19] D. Cavaliere, N. Fezans, and D. Kiehn. Method to account for estimator-induced previewed information losses - application to synthesis of lidar-based gust load alleviation functions. In *CEAS EuroGNC 2022 - Conference on Guidance, Navigation and Control*, Berlin, Germany, May. 3–5, 2022. <https://eurognc.ceas.org/archive/EuroGNC2022/html/CEAS-GNC-2022-063.html>.
- [20] C. Wallace, S. Schulz, N. Fezans, T. Kier, and G. Weber. Evaluation environment for cascaded and partly decentralized multi-rate load alleviation controllers. In *33<sup>rd</sup> Congress of the International Council of the Aeronautical Sciences (ICAS)*, Stockholm, Sweden, Sep. 4–9, 2022. [https://www.icas.org/ICAS\\_ARCHIVE/ICAS2022/data/preview/ICAS2022\\_0656.htm](https://www.icas.org/ICAS_ARCHIVE/ICAS2022/data/preview/ICAS2022_0656.htm).

## LIDAR-BASED GLA - RESULTS OBTAINED ON A GENERIC LONG RANGE AIRCRAFT CONFIGURATION

- [21] J. Hofstee, T. Kier, C. Cerulli, and G. Looye. A variable, fully flexible dynamic response tool for special investigations (varloads). In *International Forum on Aeroelasticity and Structural Dynamics (IFASD)*, Amsterdam, Netherlands, Jun. 4–6, 2003. <https://elib.dlr.de/12206>.
- [22] R. J. Guyan. Reduction of stiffness and mass matrices. *AIAA Journal*, 3(2):380, 1965. DOI: [10.2514/3.2874](https://doi.org/10.2514/3.2874).
- [23] European Union Aviation Safety Agency (EASA). *Certification Specifications and Acceptable Means of Compliance for Large Aeroplanes (CS-25) - Amendment 27*, Nov. 24, 2021.
- [24] M. R. Waszak and D. K. Schmidt. Flight dynamics of aeroelastic vehicles. *Journal of Aircraft*, 25(6):563–571, 1988. DOI: [10.2514/3.45623](https://doi.org/10.2514/3.45623).
- [25] R. L. Bisplinghoff, H. Ashley, and R. L. Halfman. *Aeroelasticity*. Dover Publications Inc., 1955. ISBN: 978-0486691893.
- [26] T. Kier and G. Looye. Unifying manoeuvre and gust loads analysis. In *International Forum on Aeroelasticity and Structural Dynamics (IFASD)*, number IFASD-2009-106, Seattle, Washington, USA, Jun. 21–25, 2009. <https://elib.dlr.de/97798>.
- [27] S. Schulz, D. Ossmann, D. Milz, T. Kier, and G. Looye. Aircraft mission simulation framework for loads analysis. In *AIAA Scitech 2020 Forum*, Orlando, Florida, USA, Jan. 6–10, 2020. DOI: [10.2514/6.2020-1620](https://doi.org/10.2514/6.2020-1620).
- [28] M. Wuestenhagen. Synthesis of a multiple-model adaptive gust load alleviation controller for a flexible flutter demonstrator. In *AIAA Scitech 2022 Forum*, San Diego, CA, USA, Jan. 3–7, 2022. DOI: [10.2514/6.2022-0440](https://doi.org/10.2514/6.2022-0440).
- [29] C. Weiser and D. Ossmann. Baseline flight control system for high altitude long endurance aircraft. In *AIAA Scitech 2022 Forum*, San Diego, CA, USA, Jan. 3–7, 2022. DOI: [10.2514/6.2022-1390](https://doi.org/10.2514/6.2022-1390).
- [30] T. Kier. An integrated loads analysis model for wake vortex encounters. In *International Forum on Aeroelasticity and Structural Dynamics (IFASD)*, number IFASD-2013-30C, Bristol, UK, Jun. 24–26, 2013. <https://elib.dlr.de/97799>.
- [31] T. Kier, R. Müller, and G. Looye. An integrated analysis model for assessment of critical load conditions for the vertical tail plane. In *International Forum on Aeroelasticity and Structural Dynamics (IFASD)*, number IFASD-2019-129, Savannah, GA, USA, Jun. 10–13, 2019. <https://elib.dlr.de/128352/>.
- [32] H. Padé. Sur la représentation approchée d’une fonction par des fractions rationnelles. *Annales Scientifiques de L’É.N.S.*, 9:3–93, 1892. DOI: [10.24033/asens.378](https://doi.org/10.24033/asens.378).
- [33] A. Khalil and N. Fezans. Gust load alleviation for flexible aircraft using discrete-time  $H_\infty$  preview control. *The Aeronautical Journal*, 125(1284):341–364, 2021. DOI: [10.1017/aer.2020.85](https://doi.org/10.1017/aer.2020.85).
- [34] A. Khalil and N. Fezans. A multi-channel  $H_\infty$  preview control approach to load alleviation design for flexible aircraft. *CEAS Aeronautical Journal*, 12:401–412, 2021. DOI: [10.1007/s13272-021-00503-z](https://doi.org/10.1007/s13272-021-00503-z).
- [35] D. Cavaliere, N. Fezans, D. Kiehn, D. Quero, and P. Vrancken. Gust load control design challenge including lidar wind measurements and based on the common research model. In *AIAA Scitech 2022 Forum*, San Diego, CA, USA, Jan. 3–7, 2022. DOI: [10.2514/6.2022-1934](https://doi.org/10.2514/6.2022-1934).
- [36] D. Cavaliere and N. Fezans. Recasting discrete 1-cosine gust requirements as frequency domain specifications for load alleviation control design. In *International Forum on Aeroelasticity and Structural Dynamics (IFASD)*, Madrid, Spain, Jun. 13–17, 2022. IFASD-2022-143. <https://elib.dlr.de/193035/>.
- [37] J. Bucher. Schlussbericht für das Projekt Con-Move: Konzepte, Entwürfe und Verifikation von integrierten Movable-Funktionen. Technical report, Airbus, 2021. LuFo V.2 Con.Move - Final Report, Airbus GmbH, No. 20A1505A. DOI: [10.2314/KXP:178448878X](https://doi.org/10.2314/KXP:178448878X).

LIDAR-BASED GLA - RESULTS OBTAINED ON A GENERIC LONG RANGE AIRCRAFT CONFIGURATION

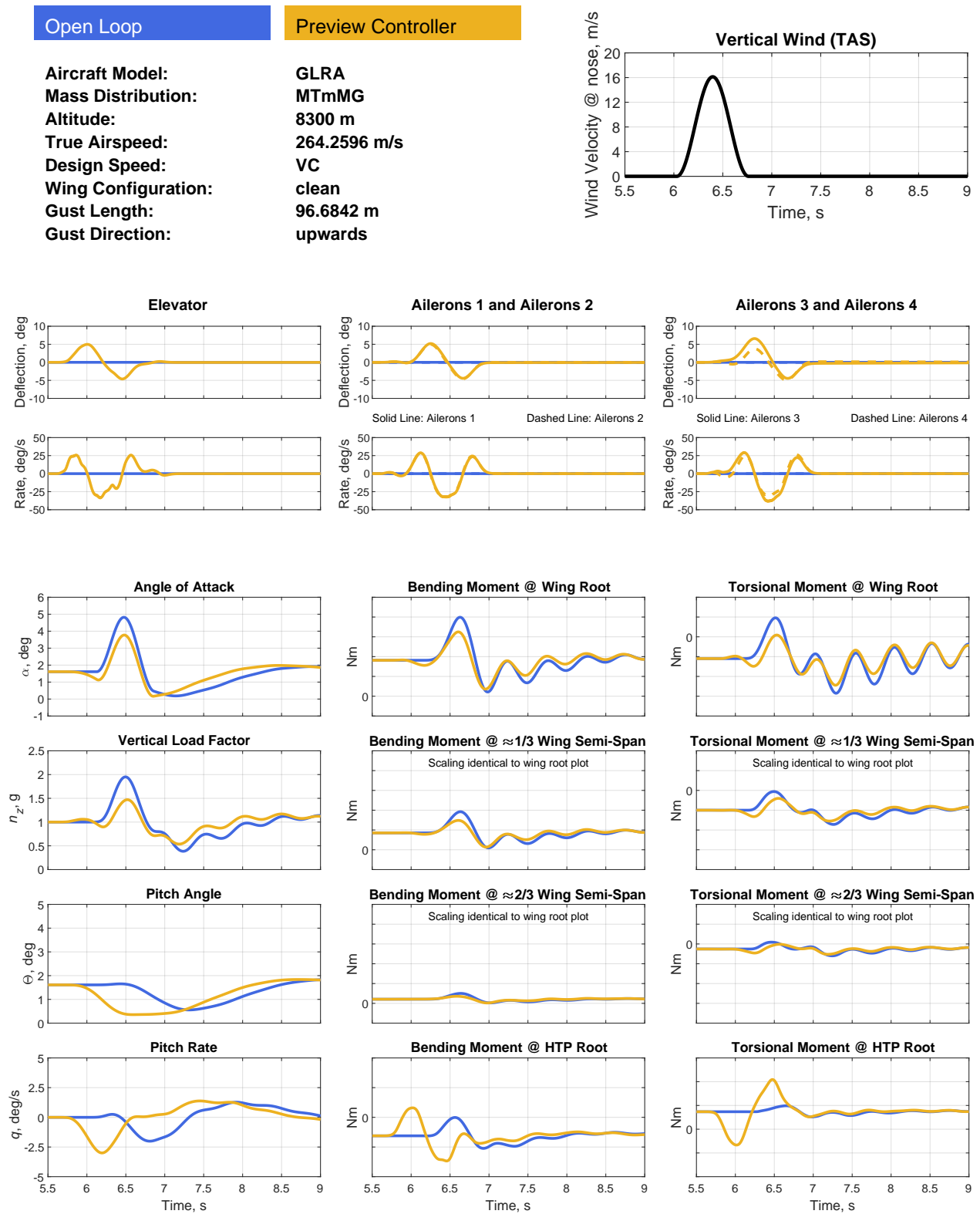


Figure 10: Time Domain Response on Gust Load Case #1: MTmMG, alt: 8300 m,  $V_C$ ,  $H = 96.6842$  m (upward)

LIDAR-BASED GLA - RESULTS OBTAINED ON A GENERIC LONG RANGE AIRCRAFT CONFIGURATION

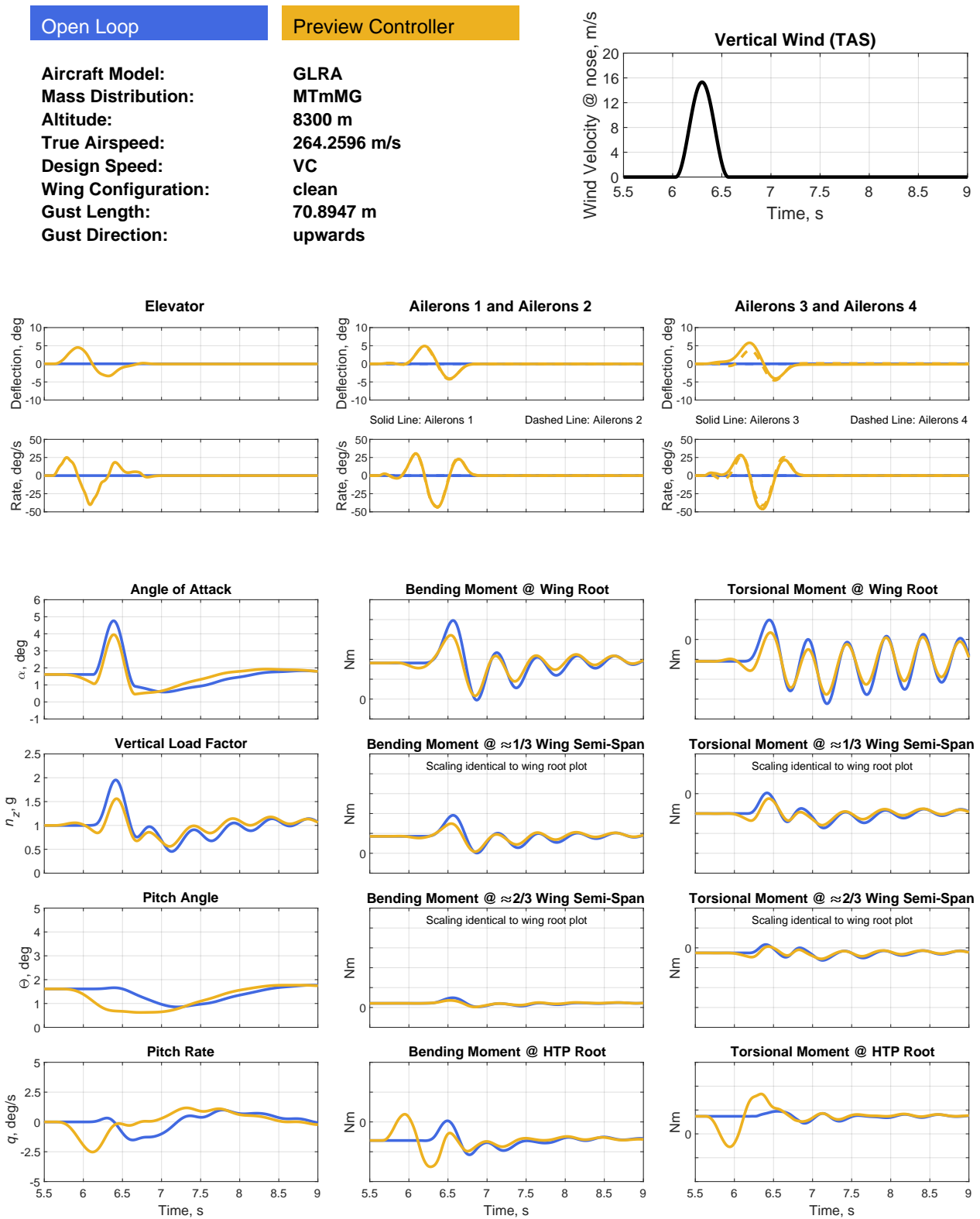


Figure 11: Time Domain Response on Gust Load Case #2: MTmMG, alt: 8300 m,  $V_C$ , H = 70.8947 m (upward)

LIDAR-BASED GLA - RESULTS OBTAINED ON A GENERIC LONG RANGE AIRCRAFT CONFIGURATION

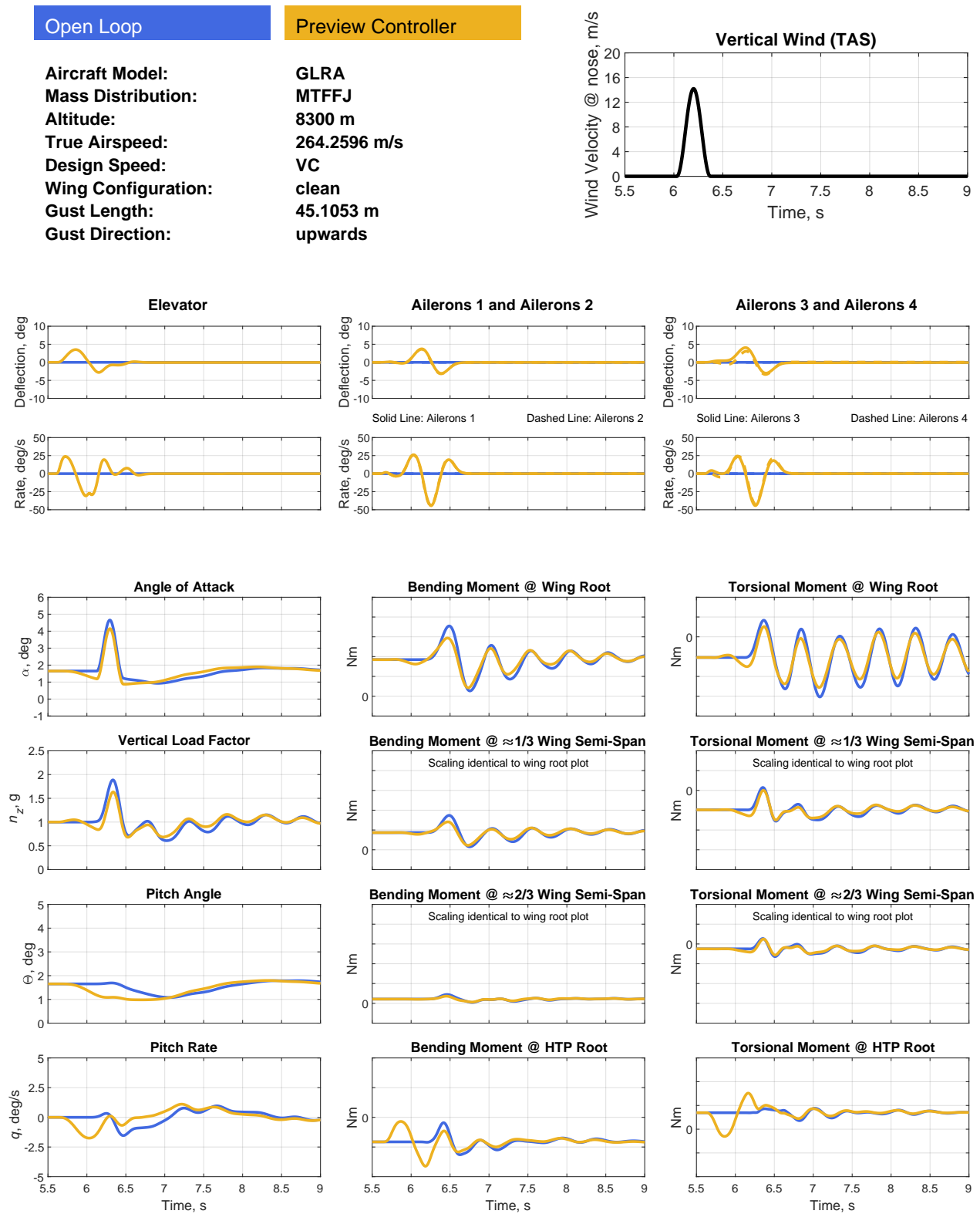


Figure 12: Time Domain Response on Gust Load Case #3: MTFFJ, alt: 8300 m,  $V_C$ ,  $H = 45.1053$  m (upward)

LIDAR-BASED GLA - RESULTS OBTAINED ON A GENERIC LONG RANGE AIRCRAFT CONFIGURATION

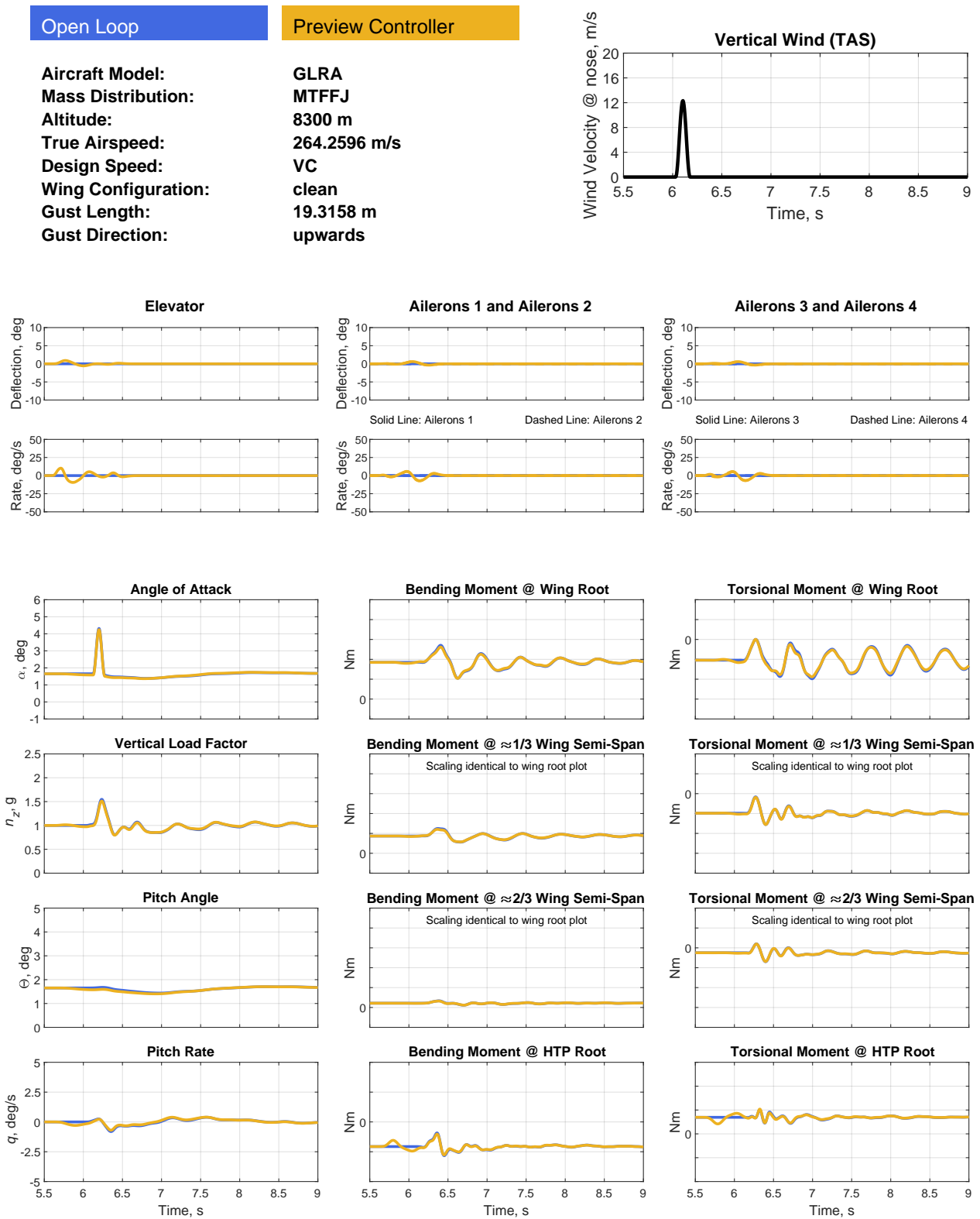


Figure 13: Time Domain Response on Gust Load Case #4: MTFFJ, alt: 8300 m,  $V_C$ , H = 19.3158 m (upward)